6

Borehole electrical panels: an experiment

M. Moreau, P. Brunel and J.-L. Mari

The Hydrogeological Experimental Site (HES) has been the subject of several studies over the past 20 years (Gaillard, 2026a). Multi-borehole logging investigations were carried out at the HES site (Audouin et al., 2008).

In this chapter, we focus on the potential of vertical electrical panels installed in five open boreholes (recorded by *CPGF Horizon* in 2021), combined with optical wall imaging (carried out by *SOLEO Mesures et Développements* in 2005 and *SEMM Logging* in 2006), to detect karst networks.

In 2021, as part of the KARST'OGENE project, *CPGF Horizon* carried out measurement campaigns on the HES. These investigations included hydrogeological tracer studies (see Chapter 7, Boulais et al. 2026) and vertical electrical panels. The objectives of the KARST'OGENE project were as follows:

1. to test and validate measurement methods and equipment on a well-documented hydrogeological site, with a view to applying them to applied hydrogeology projects;
2. to verify mass transfer between the various horizontal karst levels intersected by the HES boreholes, using convergent radial tracers.

Following the 3D seismic survey, Mari and Porel (2008) identified 3 main porous layers at depths of 35-40, 85-87, and 110-115 m that turned out to be karstic levels.

DOI: https://doi.org/10.1051/978-2-7598-3934-6.c006

The primary objective of the electrical resistivity panels was to investigate the electrical signature of these layers.

Vertical resistivity panels were implemented in five boreholes: M20, M04, M08, M07, and M11 (Fig. 1).

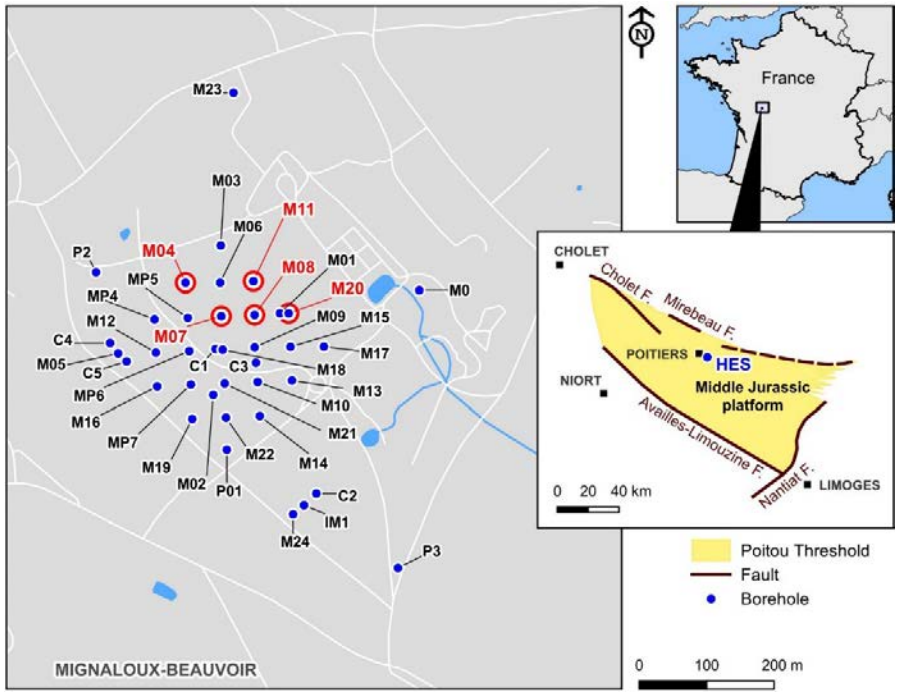

Figure 1 *Location of boreholes at the Poitiers HES site, France. Red circles indicate the boreholes selected for electrical measurements.*

Material and method

Electrical prospecting (Chapellier, 2001a) is a non-destructive geophysical method used to determine the structure and quality of the terrain. This method is based on the ability to represent the nature of the terrain in terms of one of its physical parameters: electrical resistivity.

The resistivity of geological formations primarily depends on the following factors:

- water and clay content;
- composition of electrically conductive minerals, such as sulfides (pyrite, galena), iron oxides, graphite, gold, and silver.

In boreholes, the Electrical Cylinder Method (Lantier & Frappin, 2000), developed by Soldata Geophysic (now known as Sixense Geophysics), is a technique

that enables radial investigation around boreholes (Habert et al., 2006). Today, this method has been adapted and is commonly used in geotechnical applications to measure the diameter of jet grouting columns (Frappin et al., 2001; Frappin, 2011).

At the HES site, a similar method was used, involving transmitting and receiving electrodes placed within the borehole to measure variations in electrical potential. Data processing focused exclusively on apparent resistivity values. As part of the KARST'OGENE project, vertical electrical panels were incorporated to assess the detectability of karst horizons by comparing the results with existing data.

The vertical electrical panels were performed using the following equipment:

- a 132-meter cable lowered to the desired depth in the boreholes, holding 32 electrodes spaced at 1-meter intervals.
- an ABEM Terrameter LS2 resistivity meter.

(a)

(b)

Figure 2 *View of measurement equipment. (a) Electrode on measuring cable, (b) ABEM Terrameter LS2 resistivity meter.*

A Wenner-Schlumberger measurement protocol was used from the bottom to the top of the open-hole sections of the boreholes, with offsets of 15 m for each roll-along measurement performed.

For each measurement, one set of 4 electrodes out of the 32 is used. Two electrodes are used for current injections (A and B), and two for measuring the electrical

potential (M and N). The greater the spacing between the quadruplet of electrodes (A and B, M and N), the thicker the slice of ground surveyed around the borehole.

Using this quadrupole configuration for surface measurements, the apparent resistivity ρ_a (in Ohm·m) of the ground through which the current flows is calculated using the following formula:

$$\rho_a = K \Delta V / I$$

With I the current intensity, ΔV the potential difference between electrodes M and N, K a geometric factor depending on the electrode arrangement:

$$K = 2\pi \times (1/AM - 1/AN - 1/BM + 1/BN)^{-1}$$

The factor 2π is used for surface measurements, as it represents the half-sphere of current displacement around the injection electrodes. This half-sphere is the result of the electrode positioning at the interface between two media:

- the ground, through which the current propagates.
- the infinitely resistant air, where the current does not propagate.

In a vertical borehole, the acquisition device is placed inside the well. The contact between the electrodes and the formation is indirect, occurring through the borehole fluid, which is typically either a water-based drilling mud or fresh water. The resistivity of fresh water generally ranges from 10 to 1000 ohm·m, depending on factors such as ionic concentration, temperature, and the presence of dissolved solids. For water-based drilling muds, resistivity typically ranges from a few ohm·m to around ten ohm·m, depending on salinity and temperature.

The apparent resistivity equation for a borehole configuration is similar to that used in surface measurements but must take into account the cylindrical geometry of the medium. In certain idealized cases—such as a narrow borehole within a homogeneous formation—apparent resistivity can be approximated using a formula analogous to that of surface configurations, with an adapted geometric factor K. This factor depends on electrode spacing, the relative position of the electrodes in the well, borehole diameter, borehole fluid properties, and the geological model.

The borehole resistivity profile is then obtained by successively combining different quadrupoles along the measurement cable, with each electrode alternately playing the role of current injection or measurement (Fig. 3).

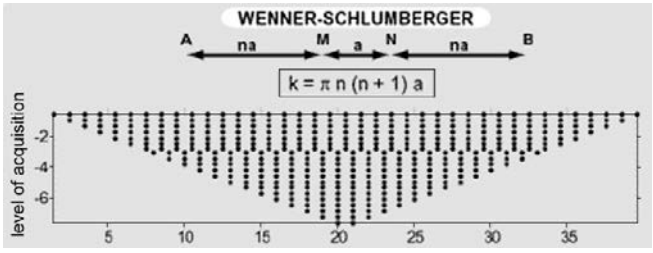

Figure 3 *Electrical resistivity measuring devices based on a Wenner-Schlumberger scheme, with a = MN (m) separation and n = acquisition data level (after D. Chapellier, 2001a).*

Acquisition

The five electrical resistivity panels produced are shown as apparent resistivities in Figure 4.

According to the porous levels identified by Mari and Porel (2008):

- the 30-meter depth level could not be studied, as electrical measurements in the boreholes only started at best at 35 meters for panels M04 and M20;
- the 50-meter depth level was studied for panels M04 and M20;
- the 85-meter depth level is covered by all five vertical panels;
- finally, the 115-meter depth level is covered by all panels except M04, which ends at 105 meters.

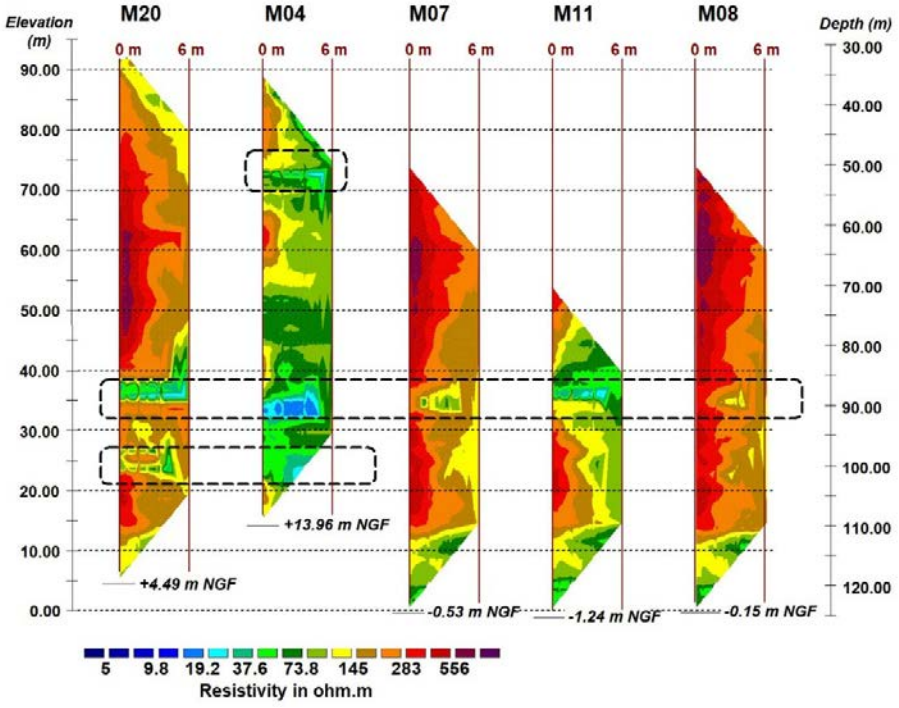

Figure 4 *Vertical resistivity panels measured from boreholes M20, M04, M07, M11, and M08. Dotted boxes indicate the location of karstic levels.*

Figure 5 presents a comparison between electrical resistivity measurements obtained from long normal logs (Chapellier, 2001b) and those from the electrical panels.

In the electrical panels, the apparent resistivity of the limestones is generally above 180 ohm·m down to approximately 110 meters. An exception is observed in panel

M04, where apparent resistivities remain lower throughout the entire depth range. Below 110 meters, apparent resistivities in boreholes M20, M07, M08, and M011 drop below 100 ohm·m.

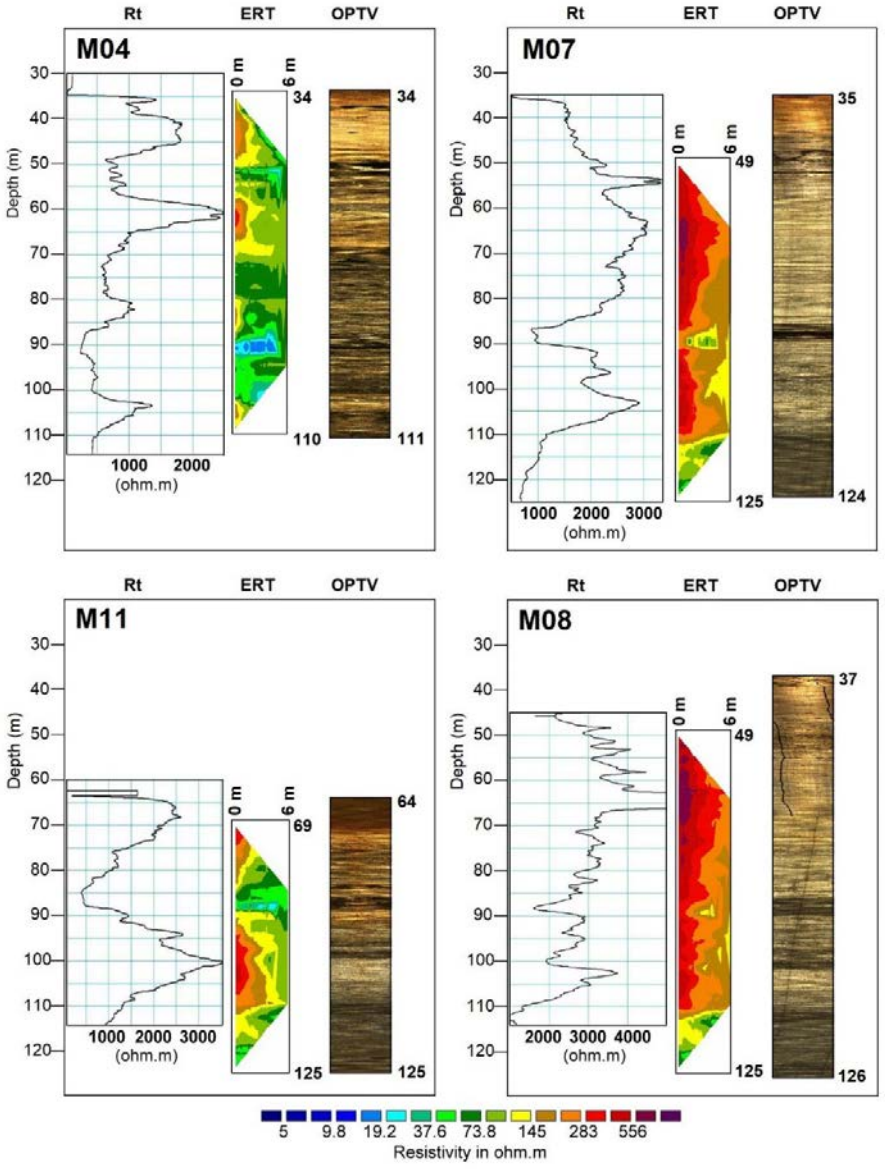

Figure 5 *Comparison of measured resistivities (long normal logs vs. ERT resistivity panels) with OPTV images for boreholes M04, M07, M08, and M11. For each borehole, from left to right: long normal resistivity log (Rt), ERT resistivity panel, and optical televiewer image (OPTV).*

The lower resistivity values observed in the electrical panels, compared to those obtained from longnormal Rt logs, arise both from the choice of the geometric factor K and, more importantly, from the effect of the borehole fluid (its conductivity), which conducts current and substantially influences the measurements. However, if the borehole geometry remains constant (i.e., the diameter does not vary) and the borehole fluid properties are unchanged, then for a given electrode configuration, the influence of the borehole fluid remains consistent at all depths. Under these conditions, relative variations in apparent resistivity still offer valuable insights for geological interpretation.

A GFTC tool, which simultaneously records Gamma Ray, Flow, Temperature, and Water Conductivity logs, was run in boreholes M08, M11, and M20. The measured water conductivity averaged 500 µS/cm, corresponding to a water resistivity of approximately 20 ohm·m.

Figure 5 also illustrates the correlation between electrical resistivity measurements and Optical Televiewer (OPTV) imagery (Mari, 2026).

The optical televiewer is a downhole probe that provides a continuous, high-resolution, 360° digital unwrapped image of the borehole wall, oriented to magnetic north, using an integrated light source. It functions effectively in air or clear water and typically achieves an average resolution of approximately 2 mm, depending on borehole conditions and logging speed. In boreholes containing mud or turbid fluids, the optical televiewer must be replaced with alternative imaging tools, such as the acoustic televiewer or microresistivity imaging tools. These alternatives also generate continuous unwrapped images of the borehole wall and are extensively used for in situ mapping of natural fracture orientations, as well as for determining the orientation of the principal horizontal stress field—based on the identification of drilling-induced tensile fractures or borehole breakouts (Genter et al., 2025). In this study, the optical televiewer was deployed in boreholes with minimal karstification and long open-hole sections (M01, M09, M10, M14, M15, M17), to enable a very high-resolution hydro-stratigraphic analysis of the HES (Gaillard, 2026b).

In boreholes M07, M08, and M11, low resistivity values identified by resistivity logs (Rt and ERT) are correlated with dark zones on the OPTV images between 85- and 90-meters depth. In borehole M04, a conductive horizon is observed between 50.05 and 53.15 meters, where a sequence of vertically stacked cavities—up to 1 meter in height—is clearly visible on both the OPTV and Rt resistivity logs.

Geological Interpretation

Each borehole is presented in a summary figure that, from left to right, compiles four pieces of information (Fig. 6, 7, and 8):

- vertical electrical resistivity panel (ERT),
- optical Televiewer image (OPTV),

- geological description derived from cuttings analysis during drilling (Bernard, 2005),
- associated geological layers (general stratigraphy).

All electrical resistivity measurements were taken in the open hole section of the boreholes.

In borehole M20 (Fig. 6), the open-hole section begins with partially altered oolitic limestone extending down to 56 m. Below this depth, the formation transitions into dolomitized limestone containing several flint layers. The boundary between the oolitic and dolomitic limestones is clearly distinguishable on the OPTV images due to a change in coloration. The OPTV also reveals two dark zones, between 85–89 m and 96–102 m, which correspond to voids that were not identified in the cuttings log.

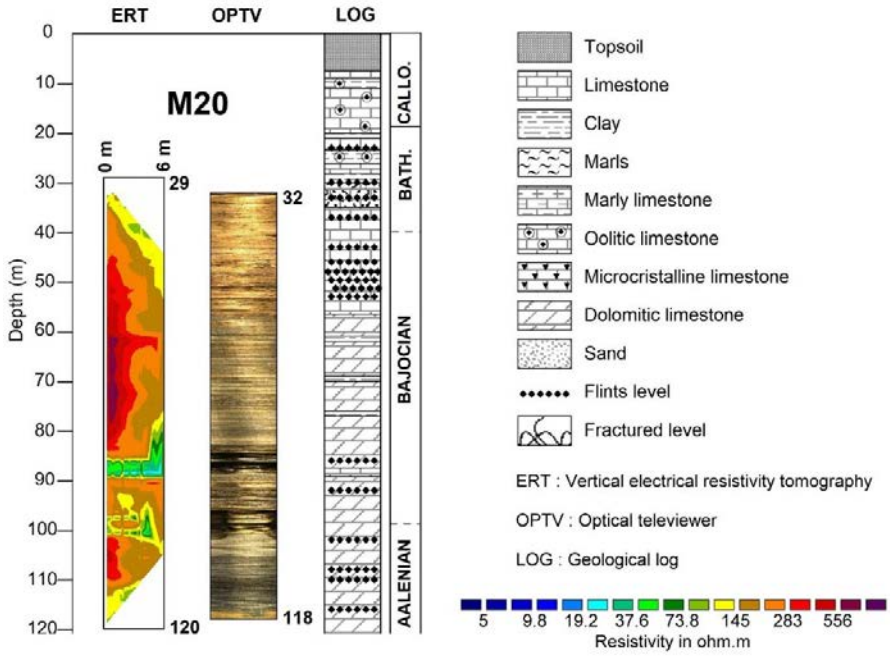

Figure 6 *Comparison of measured resistivities with available geological data for borehole M20. From left to right: vertical electrical resistivity tomography (ERT), optical televiewer (OPTV), geological log (LOG).*

The vertical resistivity profile indicates that the Dogger limestones are generally resistive (ρ_a >150 ohm·m). However, three lower resistivity anomalies are present. Two of these coincide precisely with the voids observed on the OPTV, while the third is located near the base of the borehole, at a depth of less than 110 m.

In borehole M04 (Fig. 7), the open-hole section begins with oolitic limestone down to a depth of 49 m. Below this, the cuttings log describes a succession of clayey and marly layers within the Bajocian formation. Compared to M20, the OPTV data from M04 reveal generally darker intervals, reflecting the clayey-marly nature of the limestone. The first clayey interval, described between 49 and 53 m in the cuttings log, corresponds to a karstic void observed on the OPTV. Two additional karstic zones are identified on the OPTV at depths of 70 m and 91 m.

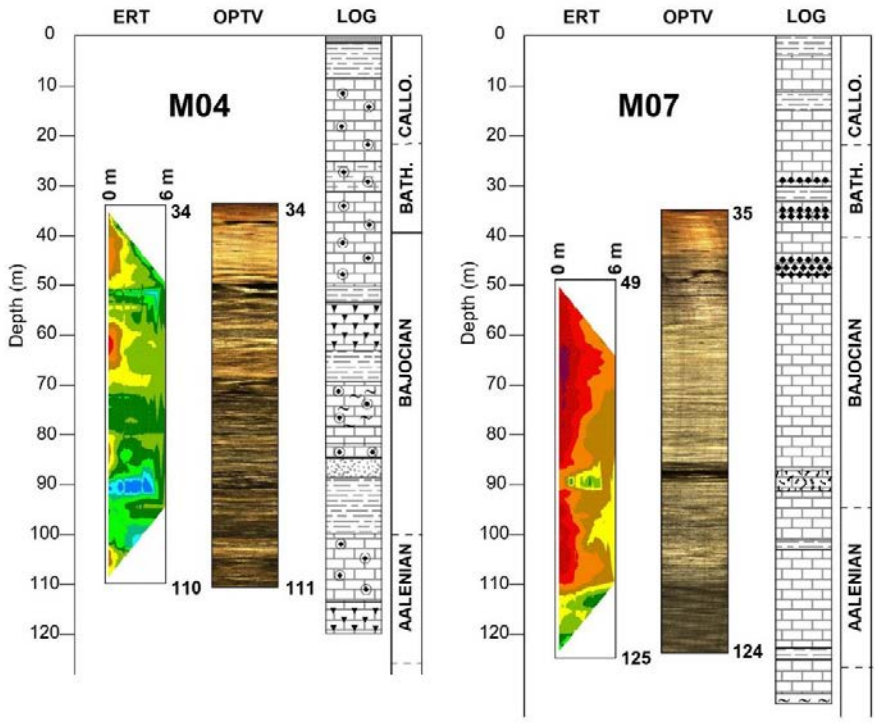

Figure 7 *Comparison of measured resistivities with available geological data for borehole M04 and M07. Refer to Figure 6 for the ERT resistivity color scale. From left to right: vertical electrical resistivity tomography (ERT), optical televiewer (OPTV), geological log (LOG).*

Electrical resistivity tomography (ERT) indicates that the limestone in this section has relatively low resistivity values, often below 100 ohm·m, which aligns with the clayey-marly composition described in both the cuttings log and the OPTV imagery. Two horizontal zones of very low resistivity are detected at the karstic levels observed on the OPTV at 49–53 m and 91 m.

In borehole M07, the cuttings log indicates limestone throughout the open-hole section, with a fractured zone around 90 m and clay-rich intervals at depths of 104 m and 124 m. The OPTV imagery reveals well-indurated limestone over most

of the open-hole section. A darker interval is observed between 86 and 90 m, corresponding to a karstic zone. From a depth of 110 m onward, the OPTV shows a general darkening, suggesting increased clay content or alteration.

The electrical resistivity tomography (ERT) data show high resistivity values (ρ_a >150 ohm·m) down to approximately 110 m, consistent with compact limestone. Below this depth, resistivity decreases (ρ_a <150 ohm·m), reflecting the presence of clay or increased porosity. A single horizontal low-resistivity anomaly is detected at 90 m, matching the karstic level observed on the OPTV between 86 and 90 m.

In borehole M11, the cuttings log indicates limestone interbedded with clayey layers within the Bathonian and Bajocian formations. This is reflected in the OPTV imagery, which generally appears dark, except for a lighter interval between 100 and 110 m. A very dark zone is visible on OPTV between 86 and 89 m, corresponding to an open and highly fractured level. Interestingly, this interval is described as a clay layer in the cuttings log.

The ERT profile shows relatively low resistivity starting from a depth of 110 m. Between 90 and 110 m, the resistivity is slightly higher but remains lower than in

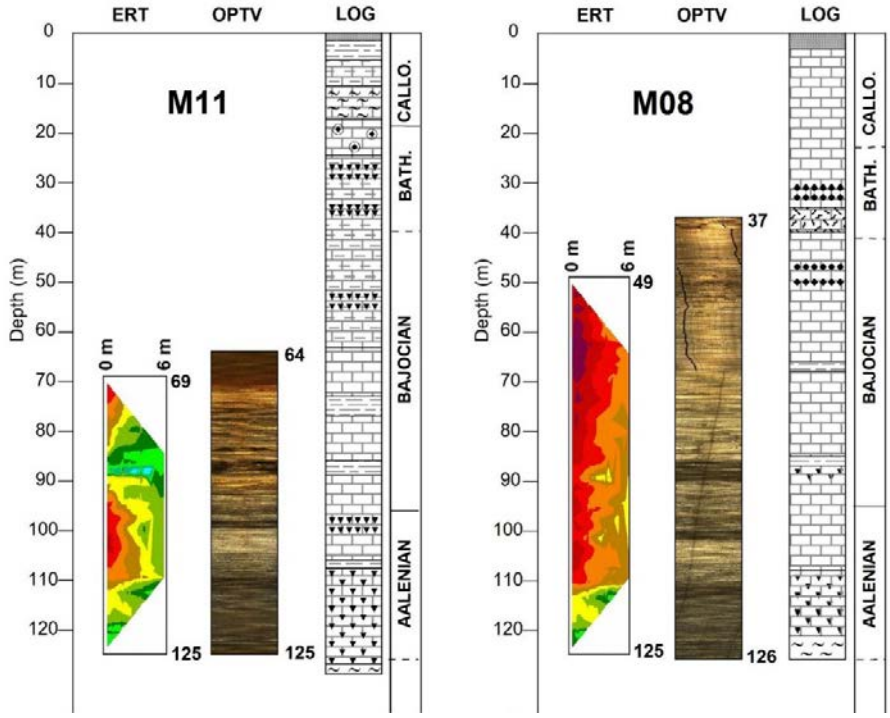

Figure 8 *Comparison of measured resistivities with available geological data for boreholes M11 and M08. Refer to Figure 6 for the ERT resistivity color scale. From left to right: vertical electrical resistivity tomography (ERT), optical televiewer (OPTV), geological log (LOG).*

boreholes M07, M20, and M08, suggesting a higher clay content in the limestone consistent with the cuttings log and OPTV observations. A distinct low-resistivity anomaly is observed between 86 and 89 m, corresponding precisely to the fractured zone identified on the OPTV.

In borehole M08, the cuttings log describes Bathonian and Bajocian limestone with occasional clay layers at depths of 67 m and 86 m. The OPTV imagery reveals darker zones at approximately 90 m, 100 m, and below 110 m. However, no karstic features are observed on the OPTV.

The ERT profile indicates that the limestone is generally resistive (ρ_a >150 ohm·m), except below 110 m where resistivity decreases, likely due to increased clay content or porosity. No distinct low-resistivity anomalies are detected, which is consistent with the absence of karstic cavities intersected by this borehole.

Summary

The apparent resistivities of the limestone formations are generally greater than 150 ohm·m down to a depth of approximately 110 meters. The only exception is observed in panel M04, where apparent resistivities remain lower throughout the entire section. Below 110 meters, the apparent resistivities measured in boreholes M20, M07, M08, and M11 decrease to values below 100 ohm·m.

Lithological data obtained from OPTV imaging and cuttings logs allow for correlating the geological nature of the formations encountered in the boreholes with the ranges of apparent resistivities recorded. Apparent resistivities exceeding 150 ohm·m correspond to carbonate formations of the Upper Aalenian, Bajocian, and, to a lesser extent, Bathonian stages. The exception in borehole M04, where lower resistivities are observed in these formations, can be attributed to the more clayey-marly composition of the limestones described in the cuttings logs and evidenced by generally darker intervals on the OPTV images. The low resistivities measured at the base of the panels likely correspond to marly-limestone facies characteristic of the Aalenian.

The three main depth intervals identified by the 3D seismic block (35–40 m, 85–87 m, and 110–115 m) were clearly detected by the electrical measurements (Fig. 5). These conductive anomalies are often confirmed by OPTV images. The level located between 85 and 87 m based on seismic data is detected between 85 and 90 m by electrical methods. Comparison of resistivity panels and optical wall imagery confirms that low-resistivity point anomalies correspond to open, water-filled karst conduits.

Additionally, the karstic level identified through acoustic methods (Mari and Porel, 2018; Mari, Porel, and Delay, 2020; see also Chapter 5, Mari 2026) at approximately 100 m depth in borehole M20 is also detected by electrical panels (Fig. 6 and 9). This level exhibits a double conductive anomaly and is particularly well defined on

the OPTV images, which reveal two distinct dark corridors. The convergence of detection through acoustic, electrical, and optical wall imaging methods is noteworthy (Fig. 9).

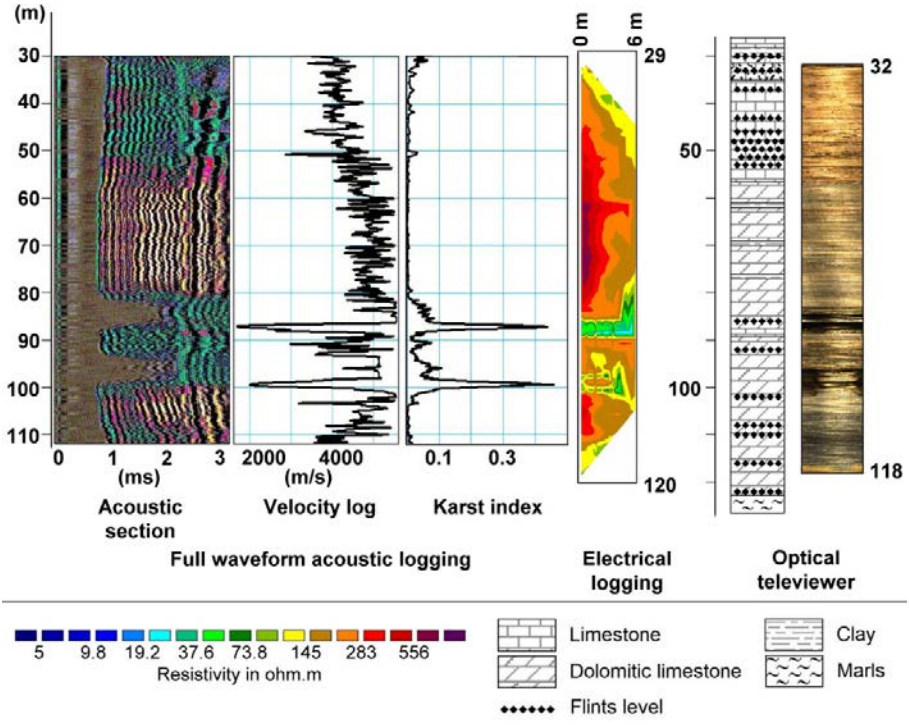

Figure 9 *Comparison of acoustic, electrical, and optical wall imaging methods in borehole M20. From left to right: the acoustic section, the velocity log, the karstic index log, the electrical resistivity panel, the geological log, the optical wall imagery*

Conclusions

The 3D seismic block acquired over the HES revealed three main high-porosity layers—presumably water-bearing—located at depths of 35–40 m, 85–87 m, and 110–115 m. These layers were identified as karstic zones. The presence of these karstic levels was clearly confirmed by both electrical resistivity measurements (Fig. 5) and Optical Televiewer (OPTV) imagery.

A comparison between the resistivity panels, long normal resistivity logs, and optical borehole images confirms that the low apparent resistivity anomalies observed in the electrical panels correspond to open, water-filled karst conduits. This correlation is particularly evident in boreholes M07 and M11.

The vertical electrical resistivity panels have demonstrated the ability to detect individual karst conduits in the Dogger limestone. When these voids are filled with water, they appear as point anomalies with low apparent resistivity. However, interpretation should always be supported by long normal resistivity logs (when available) and OPTV imagery.

References

Audouin O., Bodin J., Porel G., Bourbiaux B. (2008). Flowpath structure in a limestone aquifer: multi- borehole investigation at the hydrogeological experimental site of Poitiers, France. *Hydrogeology journal*, 16(5): 939–950. https://doi.org/10.1007/s10040-008-0275-4

Bernard S. (2005). Caractérisation hydrodynamique des réservoirs carbonatés fracturés. Application au site expérimental hydrogéologique (SEH) de l'Université de Poitiers – Ph.D. thesis, University of Poitiers, 24 November 2005.

Boulais A., Geairon H. Gaillard T. (2026). "Hydrogeological flow logging and dry tracer tests", Chapter 7 in *A new concept of karst development based on hydrogeology and geophysics*, EDP Sciences. https://doi.org/10.1051/978-2-7598-3934-6.c007.

Chapellier D. (2001a). Electrical methods, from Online course of geophysics (http://www-ig.unil.ch/)

Chapellier D. (2001b). Aquifer logging course, from Online course of geophysics (http://www-ig.unil.ch/)

Frappin P., Morey J. (2001). Jet grouting column diameter measurement using the electric cylinder method, Travaux n° 775.

Frappin P. (2011). CYLJET: an innovative method for jet grouting column diameter measurement. paper EG44, EAGE Conference & Exhibition, First International conference on Engineering Geophysics, 11–14 December 2011, AI Ain, United Arab Emirates.

Gaillard T. (2026a). "Hydrogeological Experimental Site (HES)", Chapter 4 in *A new concept of karst development based on hydrogeology and geophysics*, EDP Sciences. https://doi.org/10.1051/978-2-7598-3934-6.c004

Gaillard T. (2026b). "Hydro-stratigraphic study of hydrogeological Experimental Site", Chapter 8 in *A new concept of karst development based on hydrogeology and geophysics*, EDP Sciences. https://doi.org/10.1051/978-2-7598-3934-6.c008

Genter A., Baujard C., Glaas C., Maurer V. (2025). "Towards a revisited geothermal conceptual model in the Upper Rhine Graben", Chapter 4 in *Geophysics in geothermal exploration: a review*, EDP Sciences, https://doi.org/10.1051/978-2-7598-3752-6.c004

Habert J., Bievre G., Zumbo V. (2006). Optimization of geophysical methods for the old mining galleries, in National Geotechnical and Engineering Geology Day – JNGG' 2006 Lyon (France): 17-24.

Lantier F., Frappin P. (2000). Method and apparatus for probing and inspecting an underground volume, patent EP 0 786 673 B1, deposit number: 97106066.0, European Patent Office.

Mari J.-L., Porel, G. (2008). 3D seismic imaging of a near–surface heterogeneous aquifer: a case study, *Oil and Gas Science and Technology*, Rev IFP63: 179-201. https://doi.org/10.2516/ogst:2007077

Mari J.-L., Porel G. (2018). "Contribution of seismic and acoustic methods to the characterisation of karstic formations", Chapter 5 in *Well seismic surveying and acoustic logging*, EDP Sciences, https://doi.org/10.1051/978-2-7598-2263-8.c007

Mari J.-L., Porel G., Delay F. (2020). Contribution of Full Wave Acoustic Logging to the Detection and Prediction of Karstic Bodies, *Water,* 12(4): 948. https://doi.org/10.3390/w12040948

Mari J.-L. (2026). "Geophysical methods", Chapter 5 in *A new concept of karst development based on hydrogeology and geophysics*, EDP Sciences, https://doi.org/10.1051/978-2-7598-3934-6.c005